Analysis of Observed Streaming in Field Measurements

Hong Wang[1], Troels Aagaard[2], Lars Erik Holmedal[1] and Dag Myrhaug[1]

ABSTRACT

The analysis of velocity and suspended sediment concentration data from field measurements at Pearl Beach in New South Wales, Australia reveals the existence of onshore currents in the close vicinity of the rippled bed while the velocity is offshore directed farther up in the water column. This might be caused by wave-induced streaming beneath irregular waves over ripples. In order to test this hypothesis, a simple one-dimension vertical bottom boundary layer model capable of capturing streaming has been applied, yielding a qualitatively fair agreement between the predicted and measured mean velocity and suspended sediment concentration profiles, although the predicted suspended sediment concentration is one order of magnitude smaller. Overall, these model results support the hypothesis of the mean near-bed onshore velocity being caused by wave-induced streaming over ripples.

Keywords: Field measurements; Bedload; Ripples; Suspended sediments; Seabed boundary layer.

INTRODUCTION

The effect of streaming is important, because it contributes to the net transport of sediments and e.g. plankton and fish larvae near the sea bottom. However, seabed boundary layer streaming is not yet well understood, and is difficult to measure as it is a small (second-order) effect where the impact is observed over time. It is difficult to observe streaming under field conditions, particularly because of the frequent occurrence of bot-

[1]Dept. of Marine Technology, Norwegian University of Science and Technology, NO-7491 Trondheim, Norway. E-mail: Hong.Wang@ntnu.no.
[2]Institute of Geography and Geology, University of Copenhagen, DK-1350 Copenhagen, Denmark

tom ripples; this is further complicated by the existence of undertow and random waves.

Flow over ripples has been subjected to intensive investigations ever since the experiments by Bagnold and Taylor (1946). Recent contributions include field measurements (Traykovski et al. 1999; Traykovski 2007), measurements in large scale wave flumes (Hurther and Thorne 2011) and in oscillating water tunnels (O'Donoghue et al. 2006). The formation of 2D or 3D ripples largely depends on the sediment size with the ripples tending to be 2D for the median grain diameter $d_{50} > 0.33$ mm (O'Donoghue et al. 2006); Hurther and Thorne (2011) observed quasi-2D ripples in large scale wave flumes for $d_{50} = 0.25$ mm and found that the lee-side vortex (which contributes to the offshore transport) is stronger than the stoss-side vortex (which contributes to the onshore transport), yielding an offshore or onshore suspended sediment flux depending on the grain-size for skewed waves (van der Werf et al. 2007; Ribberink et al. 2008). Traykovski et al. (1999, 2007) found an overall offshore directed suspended sediment flux and an onshore directed bedload (ripple migration), with the net sediment transport (suspended sediment flux plus bedload) onshore directed.

Bottom boundary layer streaming occurs because of the near-bed friction leading to the horizontal and vertical velocity components (u and w, respectively) not being 90 degrees out of phase, as they are in potential flow. This implies that the time-averaged product of these velocity components (i.e. $\overline{uw}$) over a wave cycle is non-zero. Since the phase difference between u and w varies with the water depth, $\partial(\overline{uw})/\partial z$ is also non-zero and hence this term acts as a depth-dependent horizontal pressure gradient, forcing the flow in the direction of wave propagation, leading to a bottom boundary layer drift. This phenomenon was first explained by Longuet-Higgins (1953) and will thus hereafter be denoted Longuet-Higgins streaming. Also the presence of ripples and resulting vortex shedding causes $\partial(\overline{uw})/\partial z$

to be non-zero, leading to a near-bed drift velocity (see e.g. measurements Hurther and Thorne (2011) and numerical simulations by Andersen et al. (2001), Eidsvik (2006) as well as the analytical model by Davies and Villaret (1999)). Streaming caused by turbulence asymmetry in successive wave-half-cycles due to asymmetric wave forcing over a flat bed (Trowbridge and Madsen 1984; Ribberink and Al-Salem 1995; Davies and Li 1997; Holmedal and Myrhaug 2006; Scandura 2007; Holmedal and Myrhaug 2009; Fuhrman et al. 2013) or waveshape forcing (Ruessink et al. 2009; Ruessink et al. 2011; Yu et al. 2010; Kranenburg et al. 2013) has been investigated. The streaming due to asymmetric forcing alone leads to a bottom boundary layer drift against the waves (i.e. opposite to the Longuet-Higgins streaming), while the waveshape streaming imposes a bottom boundary layer drift in the wave propagation direction. Also streaming due to spatially variable roughness (Fuhrman et al. 2011) is caused by turbulence asymmetry, while streaming due to slopes is caused by both the Longuet-Higgins streaming and turbulence asymmetry (Fuhrman et al. 2009a; Fuhrman et al. 2009b; Zhang et al. 2011; Scandura and Foti 2011). Holmedal and Myrhaug (2009) and later Blondeaux et al. (2012) and Kranenburg et al. (2013) investigated the streaming and sediment transport beneath second-order Stokes waves, finding the Longuet-Higgins streaming and the streaming due to asymmetric forcing to compete.

In a previous work Aagaard et al. (2012) presented results from field experiments of sediment transport (with emphasis on bottom forms) on the shoreface of Pearl Beach, Australia. These measurements were taken outside the breakerline at water depths of 2.5-4 m beneath shoaling waves. The results included daily averaged profiles of the mean velocity, suspended sediment concentration, as well as bedload transport and ripple profiles for a pre-storm phase, storm phase and post-storm phase. For the pre-storm data the mean velocity profile was overall offshore directed over most of the water column, but in the close vicinity of the bed the velocity was onshore. Aagaard et al. (2012) explained this with the presence of bottom boundary layer streaming originally explained by Longuet-Higgins (1953). The purpose of this work is to provide a more detailed analysis of these particular field data investigating the hypothesis of streaming by using a simple seabed boundary layer model capable of capturing streaming.

FIELD MEASUREMENTS

Data were collected at Pearl Beach on the Northwest shore of Broken Bay, New South Wales, Australia during the period June 12-24, 2011. The beach has a 960 m long zeta-shaped shoreline facing the incoming ocean swell, which has a modal deep-water significant wave height of 1.5 m and spectral peak periods typically ranging from 8 to 14 s. Further details are given in Aagaard et al. (2012). Twenty-four data sets of instantaneous velocity measurements with a time resolution of 0.5 s were analysed. Each data set was taken at different tidal conditions; the duration of each set is approximately 17 minutes; the vertical resolution is 1.6 cm.

MODEL FORMULATION

The boundary layer equations have been solved numerically. The length of the flow domain equals the wave length, and the height of the domain is larger than the boundary layer thickness. In order to simplify the equations the relation $\partial/\partial\, x = -(1/c_p)\,\partial/\partial\, t$ is applied; here c_p is the wave celerity. This relation transforms the two-dimensional problem into a one-dimensional system of equations, which is easier to solve (Holmedal and Myrhaug 2009). A standard high Reynolds number $k - \epsilon$ model (subjected to the boundary layer approximations) has been adopted to provide the turbulence closure. Dirichlet conditions are used for the velocity on top of the boundary layer; at the bottom $z = z_0$ the logarithmic wall law for rough turbulent flow is applied. An equivalent wave has been applied to represent the random waves using the rms (root-mean-square) value of the measured velocity amplitude. The present model has earlier been successfully applied on seabed boundary layers (regular and random waves plus current) by Holmedal et al. (2003) and on sediment transport (Holmedal et al. 2004; Holmedal and Myrhaug 2006; Holmedal and Myrhaug 2009; Holmedal et al. 2013; Afzal et al. 2015); a convincing agreement between measurements and predictions of turbulent flow quantities and sediment concentration was obtained. The governing equations for conservation of momentum and mass are given as:

$$\frac{\partial u}{\partial t} + \frac{\partial (u^2)}{\partial x} + \frac{\partial (uw)}{\partial z} = -\frac{1}{\rho}\frac{\partial p}{\partial x} + \frac{\partial}{\partial z}(\nu_T \frac{\partial u}{\partial z}), \tag{1}$$

$$\frac{\partial u}{\partial x} + \frac{\partial w}{\partial z} = 0, \tag{2}$$

where u is the horizontal velocity component, w is the vertical velocity component, p is the pressure, ρ is the density of the water, and ν_T is the kinematic eddy viscosity.

The turbulence closure is provided by a $k-\epsilon$ model. Subjected to the boundary layer approximation, these transport equations are given by (see e.g. Rodi (1993)). Thus the governing equations are given as:

$$\frac{\partial k}{\partial t} + \frac{\partial (uk)}{\partial x} + \frac{\partial (wk)}{\partial z} = \frac{\partial}{\partial z}(\frac{\nu_T}{\sigma_k}\frac{\partial k}{\partial z}) + \nu_T (\frac{\partial u}{\partial z})^2 - \epsilon, \tag{3}$$

$$\frac{\partial \epsilon}{\partial t} + \frac{\partial (u\epsilon)}{\partial x} + \frac{\partial (w\epsilon)}{\partial z} = \frac{\partial}{\partial z}(\frac{\nu_T}{\sigma_\epsilon}\frac{\partial \epsilon}{\partial z}) + c_{\epsilon 1}\frac{\epsilon}{k}\nu_T (\frac{\partial u}{\partial z})^2 - c_{\epsilon 2}\frac{\epsilon^2}{k}. \tag{4}$$

where k is the turbulent kinetic energy and ϵ is the turbulent dissipation rate. Here Eq.(2) has been applied to write Eqs.(1), (3) and (4) in conservative form. The kinematic eddy viscosity is given by

$$\nu_T = c_1 \frac{k^2}{\epsilon}. \tag{5}$$

The standard values of the model constants have been adopted, i.e. (c_1, $c_{\epsilon 1}$, $c_{\epsilon 2}$, σ_k, σ_ϵ) = (0.09, 1.44, 1.92, 1.00, 1.30).

These equations are simplified using the relation

$$\frac{\partial \phi}{\partial x} = -\frac{1}{c_p} \frac{\partial \phi}{\partial t} \tag{6}$$

where ϕ represents u, k and ϵ; $c_p = \omega/k_p$, ω is the wave frequency, $k_p = 2\pi/\lambda$ is the wave number determined from the dispersion relation $\omega^2 = gk_p \tanh(k_p h)$, and λ is the wave length. The vertical velocity component is found from the continuity equation and is evaluated as

$$w = -\int_{z=z_0}^{z} \frac{\partial u}{\partial x} dz = \frac{1}{c_p} \int_{z=z_0}^{z} \frac{\partial u}{\partial t} dz \tag{7}$$

and inserted into Eqs. (1), (3) and (4). The integral has been evaluated numerically using the trapezoidal rule, using that $w = 0$ at $z = z_0$. A more detailed description of this model is given in Holmedal et al. (2013).

RESULTS AND DISCUSSION

Twenty-four field data sets of instantaneous velocity and suspended sediment concentration measurements with a time resolution of 0.5 s were analysed. Each of these data sets was taken at different tidal conditions; the duration of each set is approximately 17 minutes; the vertical resolution is 1.6 cm. Onshore near-bed mean velocities were found in 6 of the 24 time series. The significant wave height H_s varies between 0.64 and 0.86

m; the spectral peak wave period T_p lies between 8.1 and 9.1 s and the water depth is between 2.93 and 3.91 m; these parameters are given in Table 1. The median sand diameter is about 0.30 mm at the instrument deployment positions. It should be noted that it is a non-trivial task to determine a "fixed" bed (for model predictions) in the present case where the bedforms are moving; it is quite likely that the ripples will blur the "bed level". Here the bed level has been chosen by discarding spurious measured velocities which are obviously contaminated by moving bedforms. In the following the resulting mean profiles containing streaming will be presented.

Figure 1 shows 6 different mean velocity profiles with an onshore velocity near the bed and an offshore velocity farther away from the bed. Aagaard et al. (2012) explained this near bed onshore mean velocity with the presence of wave-induced streaming. To further test this hypothesis, the $k-\epsilon$ model (capable of capturing streaming) was applied, both with sand roughness (with a median sand diameter d_{50} of 0.32 mm and $z_0 = d_{50}/12$ for a flat bottom), and with a larger ripple roughness ($z_0 = 0.19$ cm given by $z_0 = 8\eta^2/(30\lambda_1)$ where η is the ripple height and λ_1 is the ripple length (Nielsen 1992)). An equivalent sinusoidal wave using the rms value of the near-bed wave excursion amplitude ($A_{rms} = H_s/(2\sqrt{2}\,\sinh(k_p h))$ and the spectral peak period T_p of the wave, was used to represent irregular waves. Figure 1 shows that the near-bed mean velocity profile is reasonably well predicted by the model (despite substantial underestimation of the mean velocity closest to the theoretical bed), with the "ripple-roughness" yielding the best result. This is consistent since ripples were present during measurements. Figures 1a and c show a fair model agreement for field measurement data taken from ripple mid-points while the other streaming velocities, which are underestimated, are from ripple crests possibly due to local acceleration effects. However, the fact remains that for 18 of the 24 analysed time series, either no drift was found, or the drift was offshore. A possible explanation is that these measurements are located at ripple troughs where it might be a "dead zone", i.e. no streaming. Figure 2 shows three snap shots of bottom ripple profiles for the pre-storm data analysed in the present paper; these are the only such profiles available from the pre-storm data. Clearly these profiles are highly irregular, and these are moving bedforms. It is unclear to the authors whether particular realizations of such irregular ripple forms could cause a near-bottom onshore velocity; further research, including modelling, is required. This is, however, beyond the scope of the present work.

Due to the wave action a considerable amount of the sediment transport takes place as suspended load. The existing bottom ripples are typically about 6 cm high with a ripple length of about 60 cm (although the ripples are irregular; see Figure 2). This might lead to vortex shedding over the ripples, enhancing the suspended sediment concentration. Figure 3 shows the mean suspended sediment concentration $\overline{c(z)}$ corresponding to the mean velocity profiles shown in Figures 1a-f. Overall, a log-linear profile of $\overline{c(z)}$ is observed (except a few near bed data that might be recorded in ripple troughs). Furthermore, $\overline{c(z)}$ has been predicted using an empirical formula from Nielsen (1992) valid for ripples:

$$\overline{c(z)} = C_0 e^{-\frac{z}{L_s}} \tag{8}$$

$$L_s = 1.4\eta \tag{9}$$

$$C_0 = 0.005\theta_r^3 \tag{10}$$

$$\theta_r = \frac{\theta}{(1-\pi\frac{\eta}{\lambda_1})^2} \tag{11}$$

$$\theta = \frac{\tau_{\rm b}}{\rho g(s-1)d_{50}} \tag{12}$$

where θ is the instantaneous dimensionless seabed shear stress (Shields parameter) for a sandy flat bed, $\tau_{\rm b}$ is the dimensional instantaneous seabed shear stress, g is the gravity acceleration, $s = 2.65$ is the density ratio between the sand and the water. The critical Shields parameter $\theta_c = 0.05$ must be exceeded for bedload transport to take place. Here the present $k - \epsilon$ model has been applied to obtain θ, using the empirical relation $z_0 = d_{50}/12$. Figure 3 shows that the predicted mean concentration is consistently about one order of magnitude smaller than measured, demonstrating the limitation of simple empirical sediment models applied in the field. Figure 4 shows the ratio α between the measured and modelled $\overline{c(z)}$ at $z = z_0$ plotted versus the mobility number $\psi = U_{rms}^2/(g(s-1)d_{50})$ where $U_{rms} = 2\pi A_{rms}/T_p$; the ratio varies from about 26 to 8. Here the value of the measured $\overline{c(z)}$ at $z = z_0$ have been obtained by extrapolation where we discard those few field measurement data that are not log-linear in the $\overline{c(z)}$-profile, i.e. the lowest 3 points in Figure 3a. Overall, it appears that the ratio decreases as the mobility number increases. This might be due to that the ripple heights become smaller with increasing wave activity and hence the flat bed regime is approached where the present model works well.

Figure 5 shows the mean suspended sediment flux $\overline{uc(z)}$ for the physical conditions given in Table 1. This flux is onshore for Figures 5b-f, i.e. in the same direction as the corresponding near-bed mean velocities shown in Figure 1. However, the flux in Figure 5a is offshore, i.e. opposite to the direction of the corresponding near-bed mean velocity shown in Figure 1a. As discussed in detail by, among others, by Holmedal and Myrhaug (2006) and by Fuhrman et al. (2013), $\overline{uc(z)} \neq \overline{u}\overline{c(z)}$, i.e. the mean suspended sediment flux depends on the instantaneous interaction between the suspended sediment concentration and the velocity.

The present field measurements represents complicated sediment flow, including shoaling waves, shallow water with turbulence through the entire water column, as well as irregular waves causing irregular moving bottom ripples. Moreover, there is a weak slope, and both tidal forcing and undertow are present. Overall, the onshore near-bed mean velocities shown in Figure 1 might be caused by wave-induced streaming over ripples. The fair agreement between the predicted and measured mean velocity profiles supports this hypothesis, although wave-induced streaming beneath irregular skewed waves over ripples is not yet fully understood.

SUMMARY

Velocity and suspended sediment concentration data from field measurements at Pearl Beach in New South Wales, Australia, have been analysed. The analysis reveals that although the near-bed current is overall offshore directed, there is an onshore current in the close vicinity of the rippled bed in several of the time series. This might be caused by wave-induced bottom boundary layer streaming over ripples. A simple one-dimension vertical bottom boundary layer model has been applied, yielding a qualitatively fair agreement between the predicted and measured mean velocity and suspended sediment concentration profiles, although the predicted suspended sediment concentration is one order of magnitude smaller (taking into account that these are field measurements). Hence these model results support the hypothesis of the mean near-bed onshore velocity being caused by wave-induced streaming.

Acknowledgement

This work was carried out as part of the strategical university program "Air-Sea Interaction and Transport Mechanisms in the Ocean", funded by the Norwegian Research Council.

REFERENCES

Aagaard, T., Hughes, M., Baldock, T., Greenwood, B., Kroon, A., and Power, H. (2012). "Sediment transport processes and morphodynamics on a reflective beach under storm and non-storm conditions." *Marine Geology*, 326328(0), 154–165.

Afzal, M. S., Holmedal, L. E., and Myrhaug, D. (2015). "Three-dimensional streaming in the seabed boundary layer beneath propagating waves with an angle of attack on the current." *Journal of Geophysical Research: Oceans*.

Andersen, K. H., Chabanol, M.-L., and van Hecke, M. (2001). "Dynamical models for sand ripples beneath surface waves." *Physical Review E*, 63, 066308.

Bagnold, R. A. and Taylor, G. (1946). "Motion of waves in shallow water. Interaction between waves and sand bottoms." *Proceedings of the Royal Society of London A: Mathematical, Physical and Engineering Sciences*, 187(1008), 1–18.

Blondeaux, P., Vittori, G., Bruschi, A., Lalli, F., and Pesarino, V. (2012). "Steady streaming and sediment transport at the bottom of sea waves." *Journal of Fluid Mechanics*, 697, 115–149.

Davies, A. and Li, Z. (1997). "Modelling sediment transport beneath regular symmetrical and asymmetrical waves above a plane bed." *Continental Shelf Research*, 17(5), 555–582.

Davies, A. G. and Villaret, C. (1999). "Eulerian drift induced by progressive waves above rippled and very rough beds." *Journal of Geophysical Research: Oceans*, 104(C1), 1465–1488.

Eidsvik, K. J. (2006). "Large scale modelling of oscillatory flows over a rippled bottom." *Continental Shelf Research*, 26(3), 318–337.

Fuhrman, D. R., Fredsøe, J., and Sumer, B. M. (2009a). "Bed slope effects on turbulent wave boundary layers: 1. model validation and quantification of rough-turbulent results." *Journal of Geophysical Research: Oceans*, 114(C3). C03024.

Fuhrman, D. R., Fredsøe, J., and Sumer, B. M. (2009b). "Bed slope effects on turbulent wave boundary layers: 2. comparison with skewness, asymmetry, and other effects." *Journal of Geophysical Research: Oceans*, 114(C3). C03025.

Fuhrman, D. R., Schløer, S., and Sterner, J. (2013). "RANS-based simulation of turbulent wave boundary layer and sheet-flow sediment transport processes." *Coastal Engineering*, 73(0), 151–166.

Fuhrman, D. R., Sumer, B. M., and Fredsøe, J. (2011). "Roughness-induced streaming in turbulent wave boundary layers." *Journal of Geophysical Research: Oceans*, 116(C10). C10002.

Holmedal, L. E., Johari, J., and Myrhaug, D. (2013). "The seabed boundary layer beneath waves opposing and following a current." *Continental Shelf Research*, 65(0), 27–44.

Holmedal, L. E. and Myrhaug, D. (2006). "Boundary layer flow and net sediment transport beneath asymmetrical waves." *Continental Shelf Research*, 26(2), 252–268.

Holmedal, L. E. and Myrhaug, D. (2009). "Wave-induced steady streaming, mass transport and net sediment transport in rough turbulent ocean bottom boundary layers." *Continental Shelf Research*, 29(7), 911–926.

Holmedal, L. E., Myrhaug, D., and Eidsvik, K. J. (2004). "Sediment suspension under sheet flow conditions beneath random waves plus current." *Continental Shelf Research*, 24(17), 2065–2091.

Holmedal, L. E., Myrhaug, D., and Rue, H. (2003). "The sea bed boundary layer under random waves plus current." *Continental Shelf Research*, 23(7), 717–750.

Hurther, D. and Thorne, P. D. (2011). "Suspension and near-bed load sediment transport processes above a migrating, sand-rippled bed under shoaling waves." *Journal of Geophysical Research: Oceans*, 116(C7). C07001.

Kranenburg, W., Ribberink, J., Schretlen, J., and Uittenbogaard, R. (2013). "Sand transport beneath waves: the role of progressive wave streaming and other free surface effects." *Journal of Geophysical Research. Earth Surface*, 118(1), 1–18.

Longuet-Higgins, M. S. (1953). "Mass Transport in Water Waves." *Royal Society of London Philosophical Transactions Series A*, 245, 535–581.

Nielsen, P. (1992). *Coastal bottom boundary layers and sediment transport*. Singapore, World Scientific.

O'Donoghue, T., Doucette, J., van der Werf, J., and Ribberink, J. (2006). "The dimensions of sand ripples in full-scale oscillatory flows." *Coastal Engineering*, 53(12), 997–1012.

Ribberink, J. S. and Al-Salem, A. A. (1995). "Sheet flow and suspension of sand in oscillatory boundary layers." *Coastal Engineering*, 25(34), 205–225.

Ribberink, J. S., van der Werf, J. J., O'Donoghue, T., and Hassan, W. N. (2008). "Sand motion induced by oscillatory flows: Sheet flow and vortex ripples." *Journal of Turbulence*, 9, N20.

Rodi, W. (1993). *Turbulence models and their application in hydraulics*. CRC Press.

Ruessink, B. G., Michallet, H., Abreu, T., Sancho, F., Van der A, D. A., Van der Werf, J. J., and Silva, P. A. (2011). "Observations of velocities, sand concentrations, and fluxes under velocity-asymmetric oscillatory flows." *Journal of Geophysical Research: Oceans*, 116(C3). C03004.

Ruessink, B. G., van den Berg, T. J. J., and van Rijn, L. C. (2009). "Modeling sediment transport beneath skewed asymmetric waves above a plane bed." *Journal of Geophysical Research: Oceans*, 114(C11). C11021.

Scandura, P. (2007). "Steady streaming in a turbulent oscillating boundary layer." *Journal of Fluid Mechanics*, 571, 265–280.

Scandura, P. and Foti, E. (2011). "Measurements of wave-induced steady currents outside the surf zone." *Journal of Hydraulic Research*, 49(sup1), 64–71.

Traykovski, P. (2007). "Observations of wave orbital scale ripples and a nonequilibrium time-dependent model." *Journal of Geophysical Research: Oceans*, 112(C6). C06026.

Traykovski, P., Hay, A. E., Irish, J. D., and Lynch, J. F. (1999). "Geometry, migration, and evolution of wave orbital ripples at leo-15." *Journal of Geophysical Research: Oceans*, 104(C1), 1505–1524.

Trowbridge, J. and Madsen, O. S. (1984). "Turbulent wave boundary layers: 2. second-order theory and mass transport." *Journal of Geophysical Research: Oceans*, 89(C5), 7999–8007.

van der Werf, J. J., Doucette, J. S., O'Donoghue, T., and Ribberink, J. S. (2007). "Detailed measurements of velocities and suspended sand concentrations over full-scale ripples in regular oscillatory flow." *Journal of Geophysical Research: Earth Surface*, 112(F2).

Yu, X., Hsu, T. J., and Hanes, D. M. (2010). "Sediment transport under wave groups: Relative importance between nonlinear waveshape and nonlinear boundary layer streaming." *Journal of Geophysical Research: Oceans*, 115(C2). C02013.

Zhang, C., Zheng, J., Wang, Y., and Demirbilek, Z. (2011). "Modeling wavecurrent bottom boundary layers beneath shoaling and breaking waves." *Geo-Marine Letters*, 31(3), 189–201.

Table 1: Physical parameters: H_s is the significant wave height and T_p is the spectral peak period.

Burst number	H_s (m)	T_p (s)	Water depth (m)
089	0.64	9.1	3.33
096	0.80	8.3	3.91
097	0.86	8.3	3.87
102	0.72	8.6	3.24
103	0.67	8.5	3.09
104	0.66	8.1	2.93

Figure
Click here to download Figure: Figures_ASCE.pdf

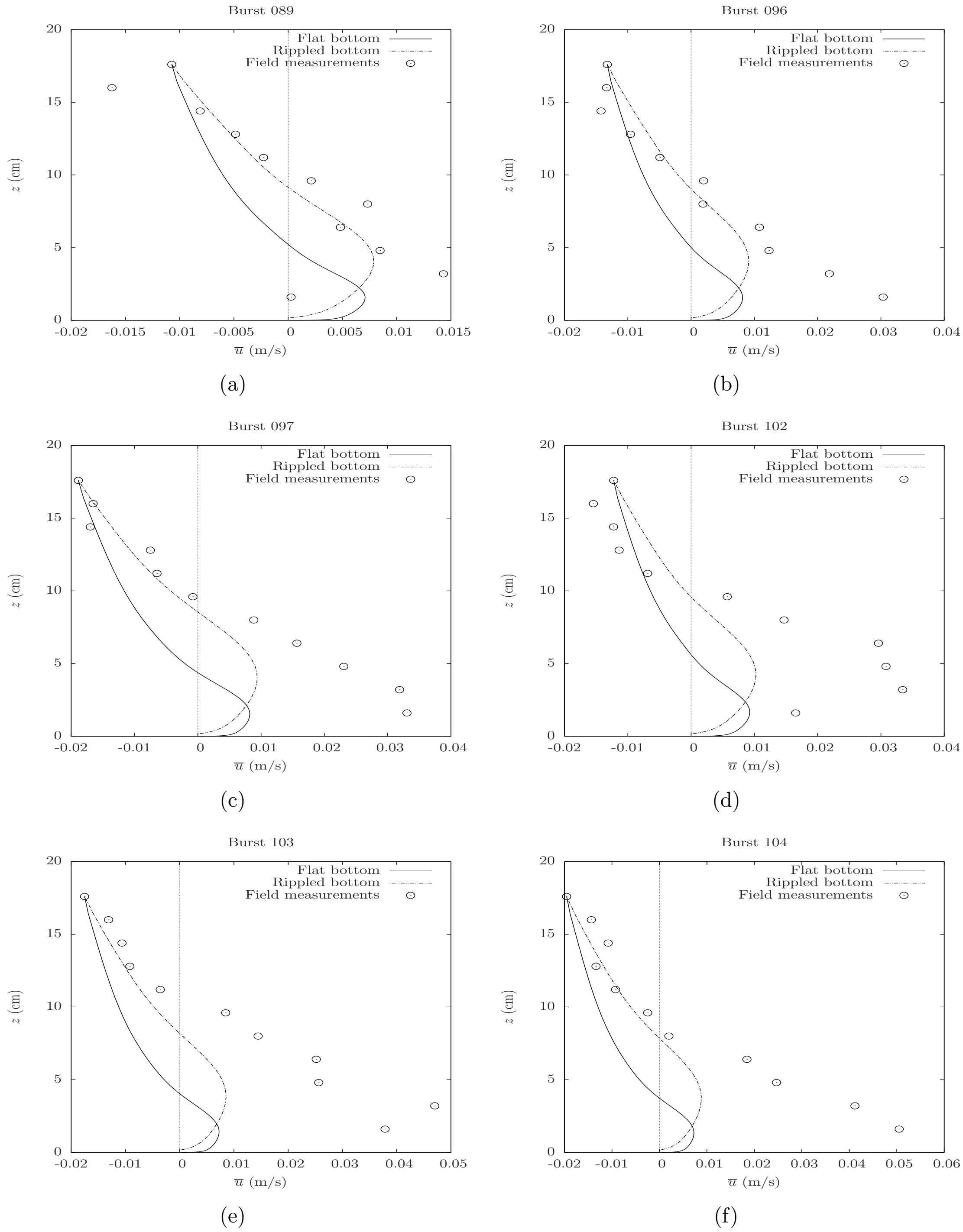

Figure 1: Mean velocity profiles $\overline{u}$ for 6 different time series, see Table 1.

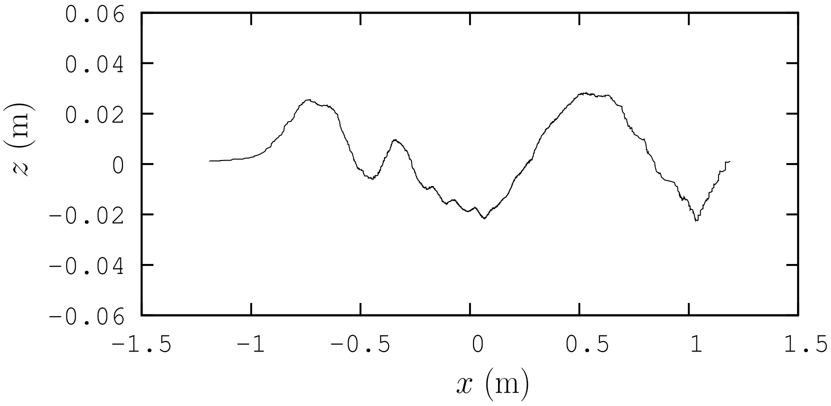

(a)

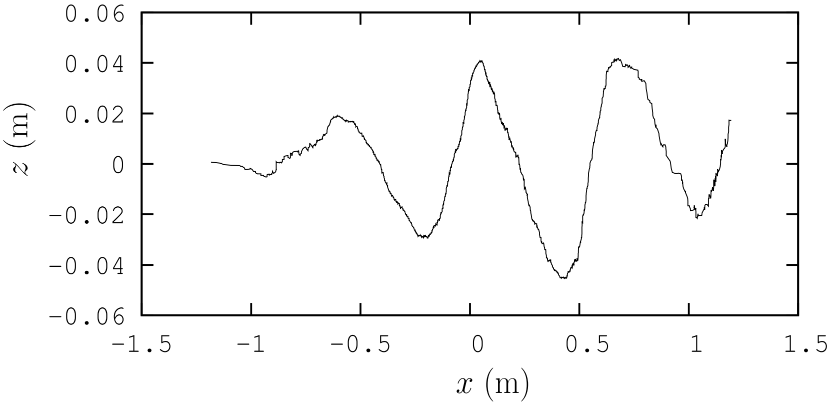

(b)

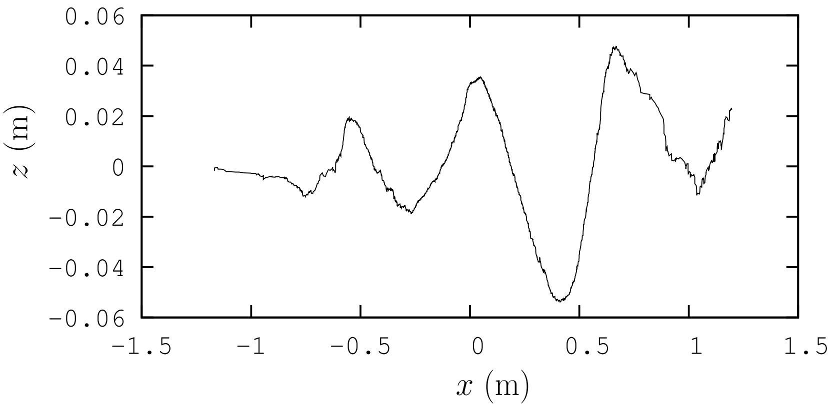

(c)

Figure 2: Three different ripple profiles

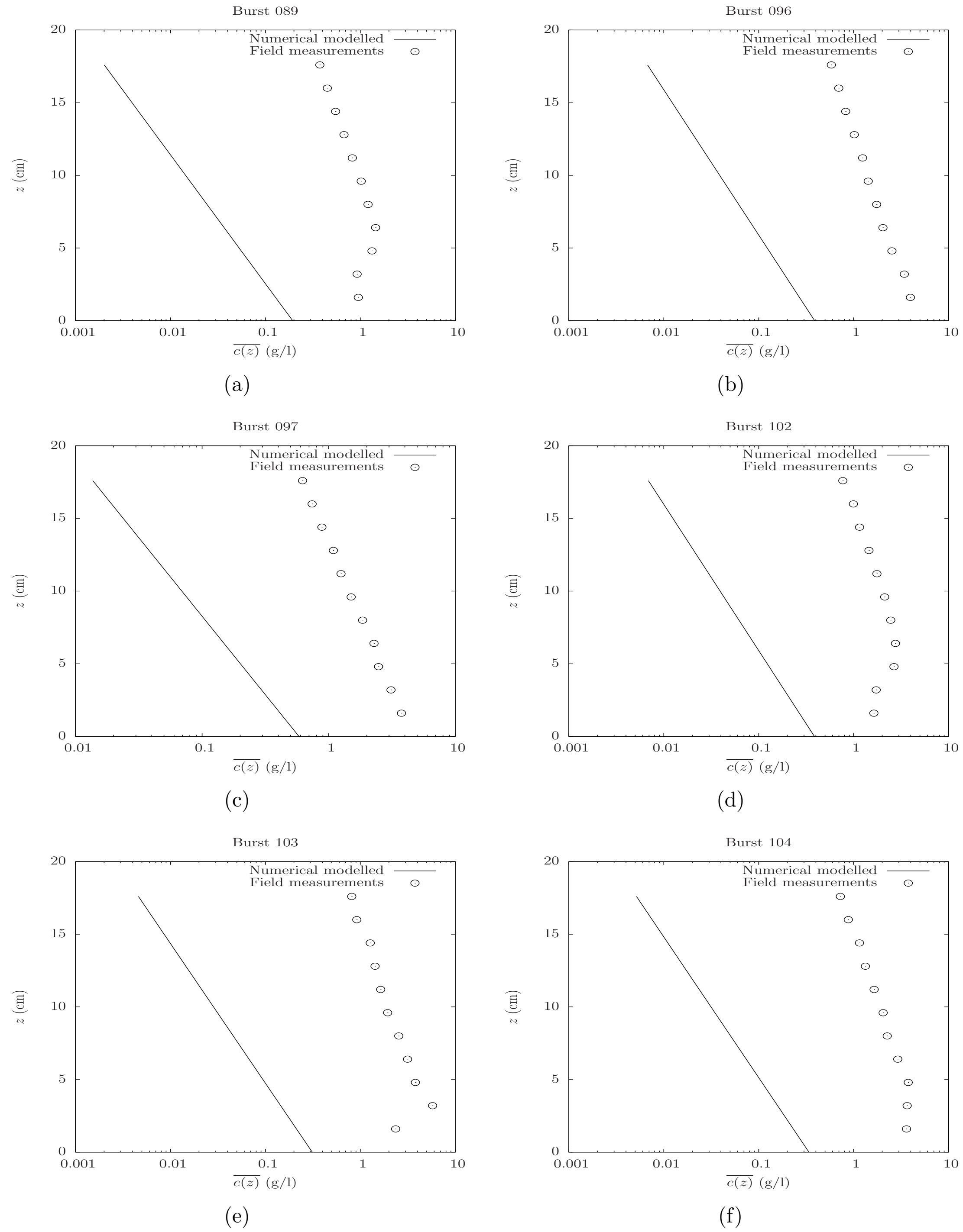

Figure 3: Mean concentration profiles $\overline{c(z)}$ for the 6 time series.

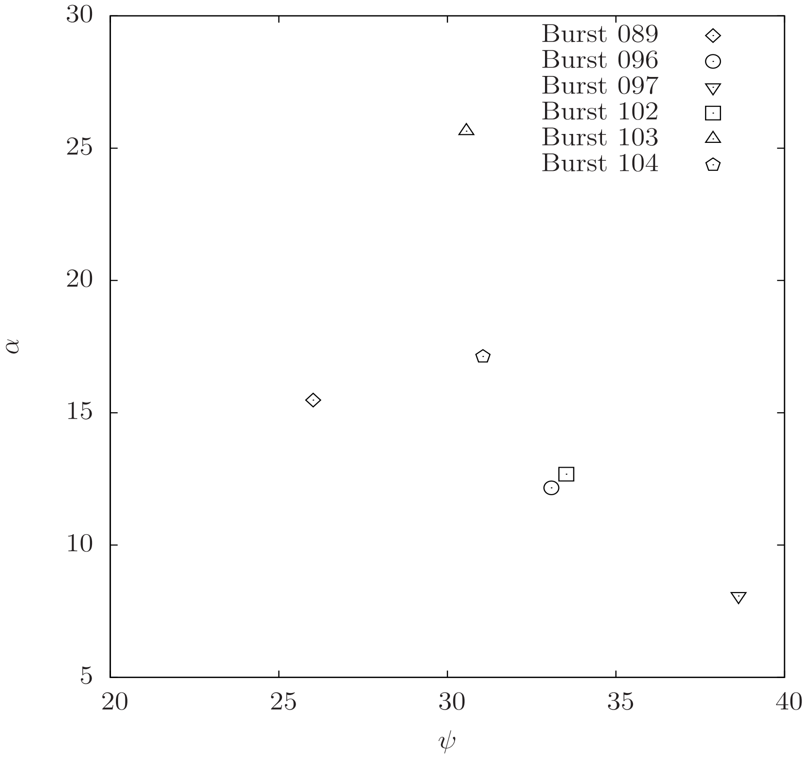

Figure 4: The ratio between the measured and modelled $\overline{c(z)}$ at the bottom versus the mobility number.

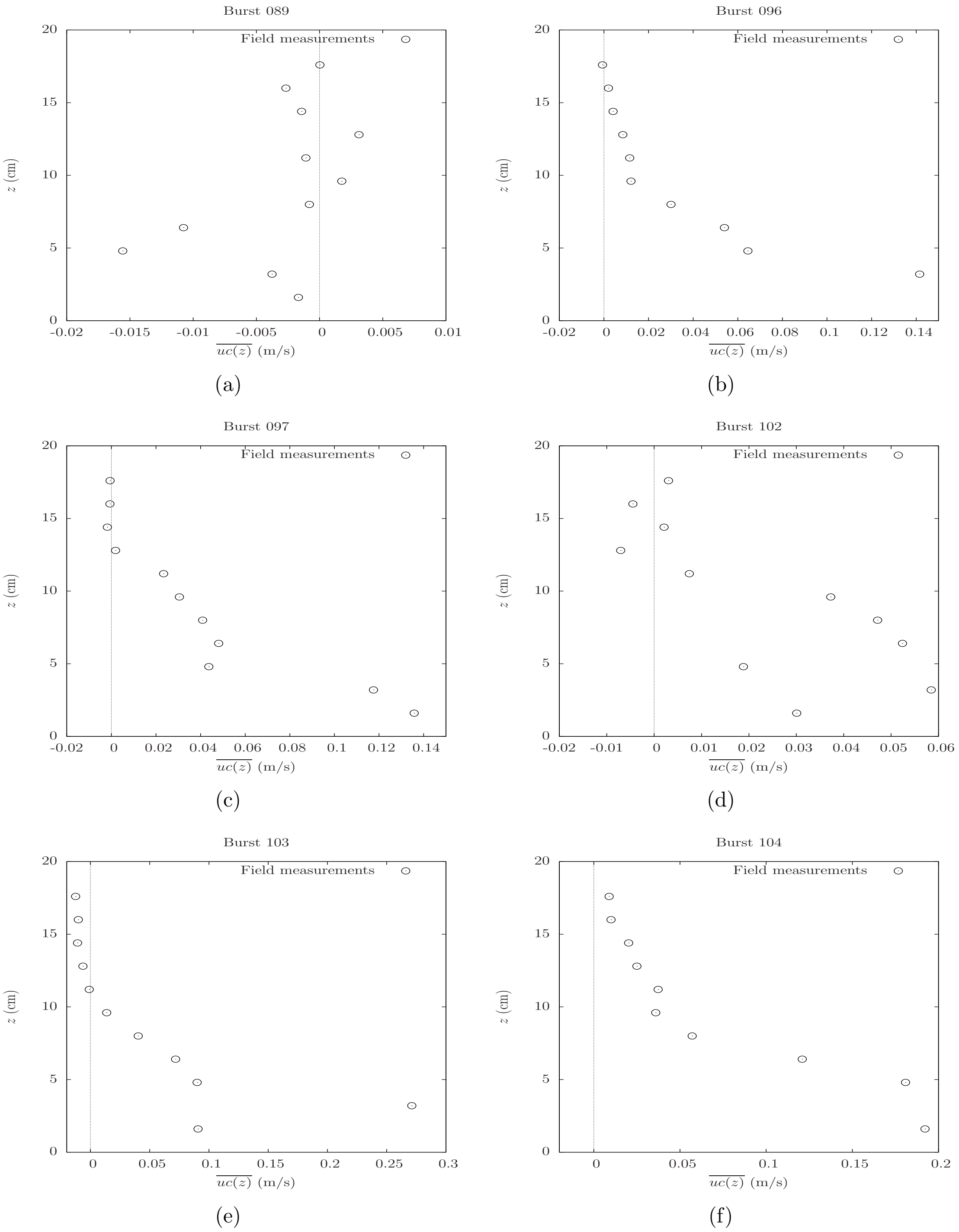

Figure 5: Mean suspended sediment flux profiles $\overline{uc(z)}$ for the 6 different time series.